7-20-2006

Spectroscopy of GRB 051111 at z = 1.54948: Kinematics and elemental abundances of the GRB environment and host galaxy

B. E. Penprase
Pomona College

E. Berger
Carnegie Observatories

D. B. Fox
Pennsylvania State University

S. R. Kulkarni
California Institute of Technology

S. Kadish
Pomona College

See next page for additional authors

Recommended Citation

Penprase, B., Berger, E., Fox, D., Kulkarni, S., Kadish, S., Kerber, L., Ofek, E., Kasliwal, M., Hill, G., Schaefer, B., & Reed, M. (2006). Spectroscopy of GRB 051111 at z = 1.54948: Kinematics and elemental abundances of the GRB environment and host galaxy. *Astrophysical Journal, 646* (I), 358-368. https://doi.org/10.1086/504678

The Astrophysical Journal, 646:358–368, 2006 July 20

SPECTROSCOPY OF GRB 051111 AT $z = 1.54948$: KINEMATICS AND ELEMENTAL ABUNDANCES OF THE GRB ENVIRONMENT AND HOST GALAXY

B. E. Penprase,[1] E. Berger,[2,3,4] D. B. Fox,[5] S. R. Kulkarni,[6] S. Kadish,[1] L. Kerber,[1] E. Ofek,[6] M. Kasliwal,[6] G. Hill,[7] B. Schaefer,[7] and M. Reed[7]

Received 2005 December 14; accepted 2006 March 23

ABSTRACT

We present a high-resolution, high S/N optical spectrum of the afterglow of GRB 051111 obtained with the HIRES spectrograph on the Keck I 10 m telescope. The spectrum exhibits three redshifted absorption systems with the highest, at $z = 1.54948$, arising in the GRB host galaxy. While the Lyα feature is outside the range of our spectrum, the high column density of weakly depleted Zn suggests that the host is a damped Lyα system with $N(\mathrm{H\ I}) \gtrsim 10^{21}(Z/Z_{\odot})^{-1}$. The bulk of the gas (>80%) is confined to a narrow velocity range of $|v| < 30$ km s^{-1}, exhibiting strong dust depletion of refractory elements such as Fe and Cr. The depletion pattern is similar to that observed in warm disk clouds of the Milky Way. We also detect absorption from all ground-level fine-structure states of Fe II, the first such example in a QSO-DLA system or GRB-absorption spectrum, which indicate conditions that are consistent with the "warm disk" depletion pattern. The absorption profiles of Fe II and Mg II extend over several hundred km s^{-1}, with a depletion pattern that more closely resembles that of QSO-DLA systems, suggesting that the sight line to GRB 051111 probes the halo of the host galaxy in addition to the dense disk. Thus, detailed diagnostics of the interstellar medium of GRB host galaxies continue to provide insight into regions that are generally missed in quasar surveys.

Subject headings: gamma rays: bursts — ISM: abundances — stars: kinematics

1. INTRODUCTION

Most of the data available for elemental abundances in the early universe come from studies of damped Lyα (DLA) systems detected in absorption against background quasars (Wolfe et al. 2005). DLA systems appear to be metal-poor, with a typical $Z \sim 0.03\ Z_{\odot}$ (Prochaska et al. 2003), and while they exhibit evidence for star formation in a few cases, the rates typically appear to be lower than in the Lyman break galaxies at a similar redshift range (Bunker et al. 1999). Recent observations have suggested the possibility, however, that higher redshift DLA systems can be associated with Lyman break galaxies (Møller et al. 2002). The DLA systems provide an unbiased estimate of mass per comoving volume of neutral gas and have provided a very useful probe of evolution of abundances at high redshifts (Nagamine et al. 2004). However, since the detection of a DLA system depends on a chance alignment of the quasar and DLA gas, some bias is introduced by the cross section for alignment, as well as the presence of dust, and these difficulties limit the QSO-DLA systems as a representative sample of the interstellar medium within the disks of early galaxies.

An alternative approach to probing intervening gas in galaxies and the intergalactic medium is to use the afterglows of gamma-ray bursts (GRBs). In the context of the relation to star formation and the nature of DLA systems, GRBs offer several advantages over quasar studies. First, GRBs are embedded in star-forming galaxies with typical offsets of a few kpc or less (Bloom et al. 2002). They therefore not only provide a direct link to star formation, but also probe the regions of most intense star formation and hence the production and dispersal of metals. Second, since the GRB afterglow emission fades away on a timescale of days to weeks, the host galaxy and any intervening DLA systems can be subsequently studied directly (e.g., Vreeswijk et al. 2004).

Third, and perhaps most important, since GRBs are likely to be located in star-forming regions within their host galaxies, this approach provides the only systematic way to directly probe the small-scale environment and conditions of star formation at high redshift; the probability of intersecting an individual star-forming cloud in a quasar sight line is vanishingly small.

Over the past several years, a few absorption spectra of GRB afterglows have been obtained, revealing relatively large neutral hydrogen column densities, in some cases with $\log N(\mathrm{H\ I}) > 22$ (Vreeswijk et al. 2004; Berger et al. 2006; Chen et al. 2005). The metallicity, inferred in only a few cases, appears to be subsolar ($Z \sim 0.01$–$0.1\ Z_{\odot}$; Vreeswijk et al. 2004; Berger et al. 2006; Chen et al. 2005; Starling et al. 2005) but with a dust-to-gas ratio that is larger than that in QSO-DLA systems (Savaglio et al. 2003). In addition, some spectra reveal complex velocity structure, interpreted as arising from ordered galactic rotation (Castro et al. 2003) and in some cases appearing to arise in the complex wind environment of the progenitor star (Möller et al. 2002; Berger et al. 2006).

In a continuing effort to characterize the interstellar medium of high-redshift galaxies and to provide a comparison to QSO-DLA systems, we present here a Keck High Resolution Echelle Spectrometer (HIRES) absorption spectrum of GRB 051111, which reveals absorption from a possible DLA system with a column density $\log N(\mathrm{H\ I}) \gtrsim 21$ at a redshift of $z = 1.54948$. The spectrum of GRB 051111 is remarkable not only for its high resolution,

[1] Department of Physics and Astronomy, Pomona College, 91711 610 North College Avenue, Claremont, CA 91711.
[2] Observatories of the Carnegie Institution of Washington, 813 Santa Barbara Street, Pasadena, CA 91101.
[3] Princeton University Observatory, Peyton Hall, Ivy Lane, Princeton, NJ 08544.
[4] Hubble Fellow.
[5] Department of Astronomy and Astrophysics, Pennsylvania State University, 525 Davey Laboratory, University Park, PA 16802.
[6] Division of Physics, Mathematics and Astronomy, 105-24, California Institute of Technology, Pasadena, CA 91125.
[7] W. M. Keck Observatory, 65-1120 Mamalahoa Highway, Kamuela, HI 96743.

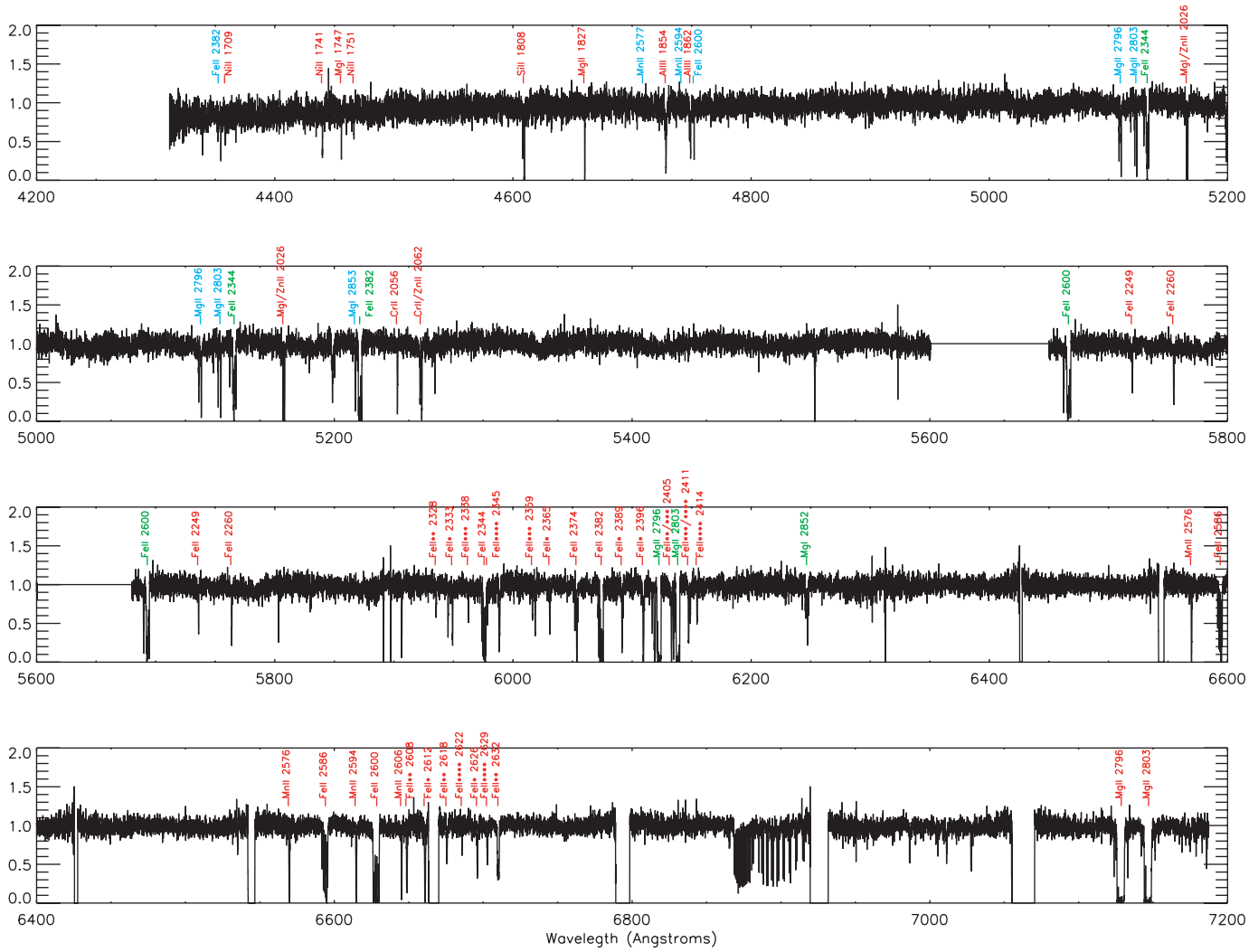

FIG. 1.—Complete spectrum of GRB 051111 obtained with HIRES on the Keck I telescope showing the spectrum of chips 1 and 2, which spans wavelengths from 4300 to 7200 Å. Absorption lines from the system at $z_1 = 1.54958$ are indicated in red, while features from the system at $z_2 = 1.18975$ are indicated in green, and those from $z_{3ab} = 0.827$ are shown in blue.

which enables accurate estimates of abundances within the host galaxy, but also for the detection and accurate measurement of excited fine-structure Fe II states (Berger et al. 2005; Chen et al. 2006) and a detailed examination of the kinematics within the interstellar medium of the host galaxy.

2. OBSERVATIONS

GRB 051111 was detected by *Swift* on 2005 November 11 at 06:00:02 UT. The duration of the burst is 47 s, and the fluence in the 15–150 keV band is $(3.9 \pm 0.1) \times 10^{-6}$ ergs cm^{-2} (Krimm et al. 2005). Observations with the ROTSE-IIIb robotic telescope started 27 s after the burst and revealed an uncataloged fading source located at $\alpha = 23^{\rm h}12^{\rm m}33\overset{\rm s}{.}2$, $\delta = +18^\circ22'29\overset{''}{.}1$ (J2000.0; Rujopakarn et al. 2005).

Spectroscopic observations of GRB 051111 were initiated at 07:03 UT, approximately 1 hr after the burst, using the HIRES mounted on the Keck I 10 m telescope (Hill et al. 2005). A total of 5400 s of exposure time were obtained using a $0\overset{''}{.}86$ wide slit at air mass 1.0–1.2. The wavelength range covered is 4200–8400 Å. Observations were coordinated by Derek Fox and Jason Prochaska and then made publicly available immediately. The spectra were reduced using the MAKEE pipeline routines (ver. 4.0.1, 2005 May), which includes optimal extraction of orders, sky subtraction, and wavelength calibration from Th-Ar arc lamp exposures, including a heliocentric velocity correction. The orders within individual frames were traced using a median combined total of the exposures, and atmospheric absorption features were removed with the Makee pipeline. A final resampling of the spectrum and continuum fitting was performed using the IRAF task `continuum`. The column densities of species detected in the spectrum were computed using a set of custom-written IDL routines for measuring equivalent widths, optical depths, and for fitting curve-of-growth models to the detected absorption species.

The spectrum, shown in Figure 1, reveals strong absorption features at a redshift $z_1 = 1.54948 \pm 0.00001$, which we interpret as the redshift of the host galaxy (see also Prochaska 2005).[8] In addition, we detect intervening systems at $z_2 = 1.18975$ (Mg II, Mg I, and Fe II), $z_{3a} = 0.82761$ (Mg I, Mg II, and Fe II), and $z_{3b} = 0.82698$ (Mg I and Mg II). The latter two most likely arise from the same object, given their close redshifts. In addition to the GRB absorption spectrum we also obtained imaging of the GRB field

[8] A GRB Coordinates Network (GCN) Circular by Prochaska 2005 provides an early statement of some salient properties of the host galaxy absorption system.

TABLE 1
Line Identification

λ_{obs} (Å) (1)	Line (Å) (2)	f_{ij} (3)	z (4)	W_0 (Å) (5)	$\log N$ (cm^{-2}) (6)
4353.26.....	Fe II 2382.7650	0.32000	0.82698	0.09582	12.58
4354.79.....	Fe II 2382.7650	0.32000	0.82762	0.13127	12.78
4358.60.....	Ni II 1709.6042	0.03240	1.54948	0.09561	13.76
4440.05.....	Ni II 1741.5531	0.04270	1.54948	0.09213	13.64
4455.97.....	Mg I 1747.7937	0.00934	1.54948	0.09585	14.36
4466.47.....	Ni II 1751.9157	0.02770	1.54948	0.08595	13.75
4607.70.....	S I 1807.3113	0.11050	1.54948	0.07275	13.09
4609.49.....	Si II 1808.0130	0.00219	1.54948	0.22796	15.77
4632.22.....	Si II* 1816.9285	0.00166	1.54948	0.03723	14.55
4660.28.....	Mg I 1827.9351	0.02450	1.54948	0.13838	14.29
4707.90.....	Mn II 2576.8770	0.35080	0.82698	0.01619	11.72
4709.55.....	Mn II 2576.8770	0.35080	0.82762	0.03428	12.02
4728.56.....	Al III 1854.7164	0.53900	1.54948	0.19586	12.97
4741.76.....	Mn II 2594.4990	0.27100	0.82762	0.02474	11.98
4749.14.....	Al III 1862.7895	0.26800	1.54948	0.13177	12.96
4750.46.....	Fe II 2600.1730	0.22390	0.82698	0.04929	12.37
4752.13.....	Fe II 2600.1730	0.22390	0.82762	0.10517	12.76
5108.88.....	Mg II 2796.3520	0.61230	0.82698	0.14426	12.43
5110.67.....	Mg II 2796.3520	0.61230	0.82762	0.22484	12.83
5122.00.....	Mg II 2803.5310	0.30540	0.82698	0.11927	12.64
5123.79.....	Mg II 2803.5310	0.30540	0.82762	0.19326	13.07
5133.24.....	Fe II 2344.2140	0.11400	1.18975	0.71346	14.09
5165.59.....	Zn II 2026.1360	0.48900	1.54948	0.19034	13.19
5214.13.....	Mg I 2852.9640	1.83000	0.82762	0.19037	12.12
5217.66.....	Fe II 2382.7650	0.32000	1.18975	1.11235	13.99
5242.38.....	Cr II 2056.2539	0.10500	1.54948	0.14935	13.46
5258.72.....	Zn II 2062.6640	0.25600	1.54948	0.17199	13.24
5267.64.....	Cr II 2066.1610	0.05150	1.54948	0.09474	13.42
5693.73.....	Fe II 2600.1730	0.22390	1.18975	1.23064	14.01
5736.02.....	Fe II 2249.8768	0.00182	1.54948	0.09490	14.80
5763.81.....	Fe II 2260.7805	0.00244	1.54948	0.13672	14.87
5935.47.....	Fe II** 2328.1112	0.03450	1.54948	0.07175	13.30
5949.25.....	Fe II* 2333.5156	0.07780	1.54948	0.15565	13.41
5962.53.....	Fe II*** 2338.7248	0.08970	1.54948	0.10608	13.08
5976.53.....	Fe II 2344.2140	0.11400	1.54948	0.37211	14.05
5978.53.....	Fe II**** 2345.0011	0.15300	1.54948	0.10861	12.84
6016.33.....	Fe II*** 2359.8278	0.06790	1.54948	0.07552	13.03
6030.93.....	Fe II* 2365.5518	0.04950	1.54948	0.13941	13.49
6053.64.....	Fe II 2374.4612	0.03130	1.54948	0.29999	14.43
6074.81.....	Fe II 2382.7650	0.32000	1.54948	0.41259	13.59
6091.62.....	Fe II* 2389.3582	0.08250	1.54948	0.19033	13.50
6109.46.....	Fe II* 2396.3559	0.31619	1.54948	0.28800	13.37
6123.31.....	Mg II 2796.3520	0.61230	1.18975	1.99290	13.93
6131.92.....	Fe II*** 2405.1638	0.02600	1.54948	0.05041	13.22
6133.08.....	Fe II** 2405.6186	0.23700	1.54948	0.25156	13.31
6139.03.....	Mg II 2803.5310	0.30540	1.18975	1.68043	14.13
6147.44.....	Fe II*** 2411.2533	0.21000	1.54948	0.18791	13.04
6148.84.....	Fe II**** 2411.8023	0.21000	1.54948	0.10497	12.68
6154.56.....	Fe II**** 2414.0450	0.17500	1.54948	0.10723	12.77
6247.28.....	Mg I 2852.9640	1.83000	1.18975	0.38539	12.24
6569.70.....	Mn II 2576.8770	0.35080	1.54948	0.23663	13.08
6594.61.....	Fe II 2586.6500	0.36933	1.54948	0.06840	14.09
6614.62.....	Mn II 2594.4990	0.27100	1.54948	0.22355	13.23
6629.09.....	Fe II 2600.1730	0.22390	1.54948	0.44168	13.75
6648.70.....	Fe II** 2607.8664	0.11800	1.54948	0.20213	13.28
6660.91.....	Fe II* 2612.6542	0.12600	1.54948	0.25575	13.50
6675.56.....	Fe II** 2618.3991	0.05050	1.54948	0.10022	13.22
6685.89.....	Fe II**** 2622.4518	0.05600	1.54948	0.04794	12.79
6696.08.....	Fe II* 2626.4511	0.04410	1.54948	0.15064	13.50
6702.78.....	Fe II**** 2629.0777	0.17300	1.54948	0.12269	12.76
6710.51.....	Fe II** 2632.1081	0.22860	1.54948	0.08600	13.40
7129.24.....	Mg II 2796.3520	0.61230	1.54948	0.55706	13.41
7147.55.....	Mg II 2803.5310	0.30540	1.54948	0.55682	13.70

Notes.—Absorption features identified in the spectrum of GRB 051111. Col. (1): Observed wavelength. Col. (2): Line identification. Col. (3): Oscillator strength. Col. (4): Redshift of the line. Col. (5): Rest-frame equivalent width. Col. (6): Logarithm of the column density assuming the optically thin case; in most cases this is a lower limit since the lines are generally saturated.

with the Echellete Spectrograph and Imager on the Keck II telescope to search for host galaxy emission as discussed in § 7.

3. KINEMATICS OF THE HOST GALAXY ABSORPTION LINE SYSTEM

The strongest absorption features in the spectrum of GRB 051111 arise from the redshift system $z_1 = 1.54948$, which exhibits a wide array of metal lines of Mg I, Mg II, Mn II, Cr II, Fe II, Zn II, Al III, Si II, Ni II, and the four ground-level fine-structure states of Fe II and one of Si II (Berger et al. 2005; Chen et al. 2006). The line identifications, observed wavelengths, and equivalent widths are listed in Table 1. Also included in Table 1 are estimates of the column densities based on the weak line limit for each transition using oscillator strengths and rest wavelengths from Morton (1991).

In Figures 2–9 we plot the absorption profiles for all transitions of the various ionic species as a function of velocity relative to the systemic redshift of $z_1 = 1.54948$. The majority of the lines exhibit a simple and symmetric structure extending from about -25 to $+25$ km s^{-1}. In addition to the narrow component absorbers, lines of Fe II and Mg II exhibit in the range of -150 to $+50$ km s^{-1} and -250 to $+170$ km s^{-1}, respectively. The absorption lines of Al III and Si II exhibit an intermediate kinematic structure with only a negative velocity extension.

The relatively low redshift precludes a direct detection of the Lyα line within the wavelength range of our spectrum, but most likely this system resembles a DLA system in its neutral hydrogen column density. In the discussion below we provide an estimate of the approximate column density of neutral hydrogen by scaling the column of weakly depleted Zn along with the average metallicity of QSO-DLA systems at a similar redshift range.

The different line profiles can be interpreted to arise from physical features in the host galaxy in the following way. First, the detection of positive velocity structure in Fe II and Mg II could arise from a burst located on the far side of the host galaxy. In this way, differential motions within the galactic rotation, as well as velocities of infalling interstellar medium (ISM) within the halo of both sides of the galaxy, would contribute absorption in both negative and positive velocity. The much larger extension at negative velocity would then arise from the disk material in the foreground of the burst, on the near side of the galaxy. If the burst is embedded at a radial position somewhere midway in the far side of the disk, the absorption would trace the complete range of negative velocities in the foreground of the burst, and a partial range of the positive velocities, since some of the disk material would be behind the burst and would be undetected in absorption.

The velocity range of $|v| \lesssim 250$ km s^{-1} is typical of the high velocity and halo gas within our Galaxy (Albert et al. 1993) and

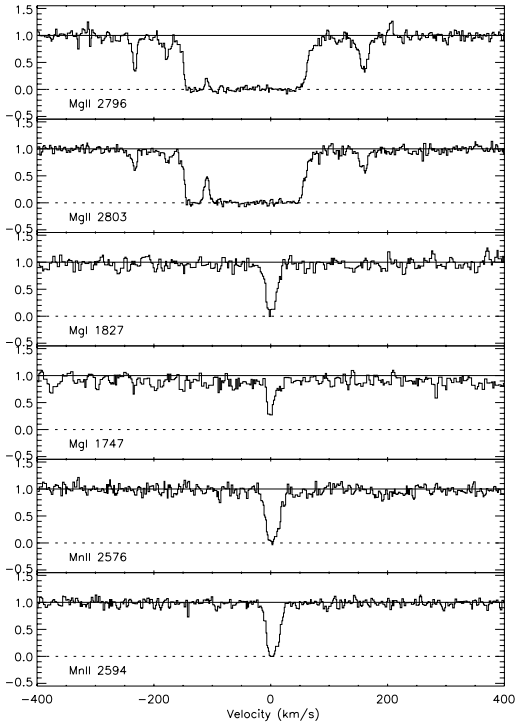

FIG. 2.—Spectrum of Mg II, Mn II, and Mg I absorption within host galaxy of GRB 051111 in the rest frame of $z_1 = 1.54948$. Observational details are given in § 2.

matches a range of velocities for quasar absorption line systems known to probe galaxy halos (Ellison et al. 2003). It is possible that some of the higher velocity absorption may arise from infall and/or outflow of metal-enriched gas. However, this interpretation is difficult to reconcile with the narrowness of the positive and negative velocity features (Figs. 2 and 5), which show line widths of $b \approx 10$ km s^{-1}.

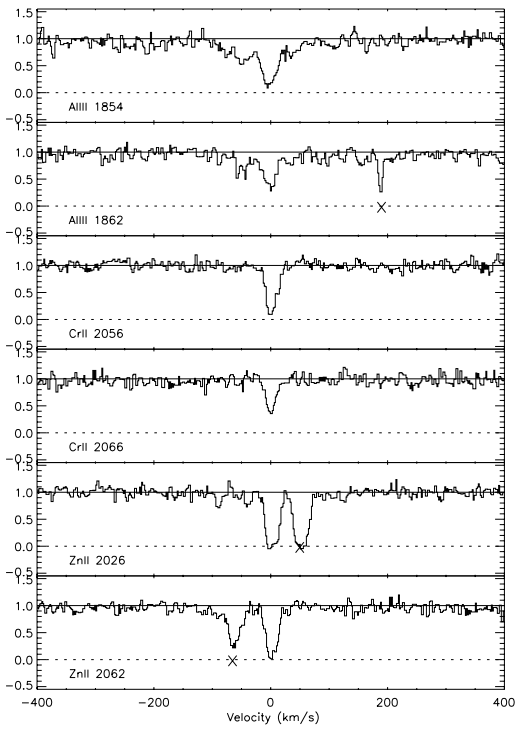

FIG. 3.—Spectrum of Al III, Al II, Cr II, and Zn II absorption within host galaxy of GRB 051111 in the rest frame of $z_1 = 1.54948$. Blended lines with other transitions are marked on the figure with crosses. Observational details are given in § 2.

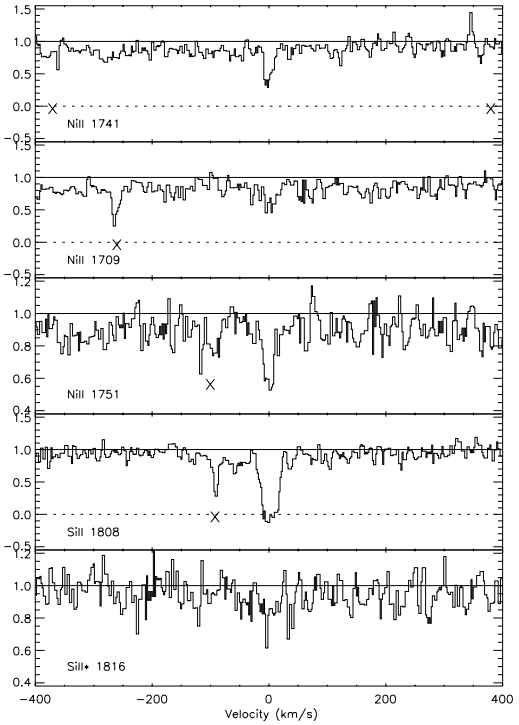

FIG. 4.—Same as Fig. 3, but for Si II, Si II*, and Ni II transitions.

On the other hand, the main absorption component centered on zero velocity is physically coincident with the burst, based on its unusual properties as derived below, and the possibility that it is actually influenced by the burst (Berger et al. 2005; Chen et al. 2006). We show that this region is unlike any that have been found in quasar spectra, but it is generally similar to absorbers in

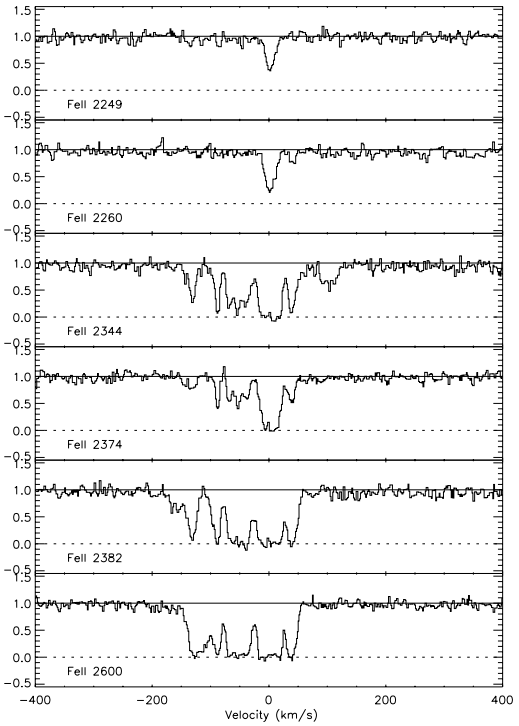

FIG. 5.—Same as Fig. 2, but for Fe II transitions. The Fe II absorption has a velocity structure similar to that of Mg II, and the large number of transitions of differing oscillator strength enables recovery of the kinematics in the dense core from -30 km s$^{-1} < v < 30$ km s^{-1}, as well as the outlying absorption from -200 km s$^{-1} < v < 60$ km s^{-1}.

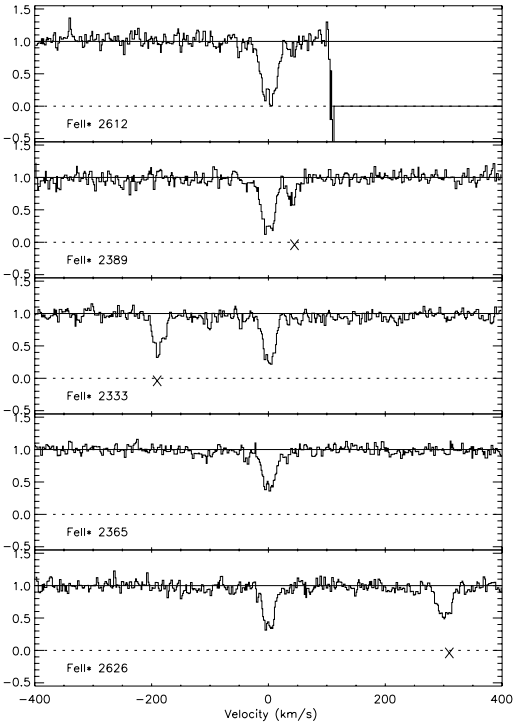

FIG. 6.—Same as Fig. 2, but for Fe II* transitions.

other GRB spectra. This suggests a fairly compact region with a cross section that is too small to be probed in quasar sight lines, most likely a molecular cloud or an individual star-forming region.

4. ELEMENTAL ABUNDANCES WITHIN THE HOST GALAXY OF GRB 051111

We employ multiple techniques for investigating in detail the abundance patterns of the narrow component centered at $v = 0$ km s^{-1} and those of the extended positive and negative velocity structures. Since some of the absorption features are saturated, we make use of a curve-of-growth (COG) analysis (Spitzer 1978), which allows us to correlate the equivalent widths

$$W_\lambda = \frac{2bF(\tau_0)\lambda}{c}, \quad (1)$$

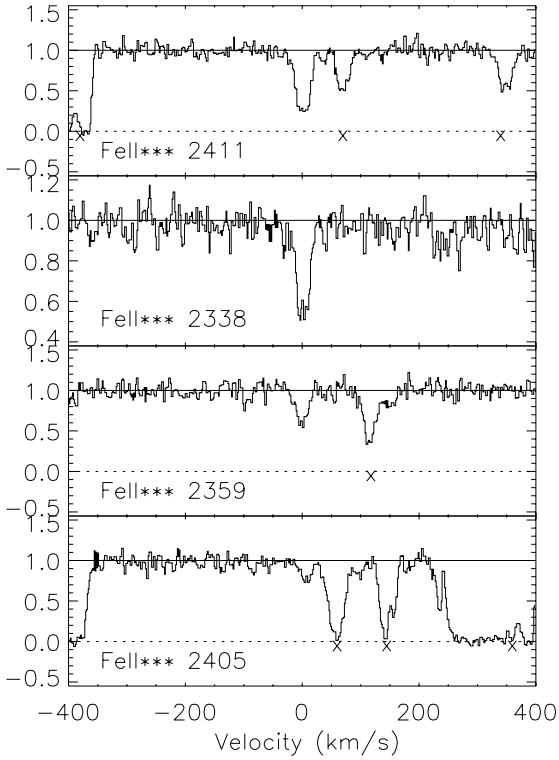

FIG. 8.—Same as Fig. 2, but for Fe II*** transitions.

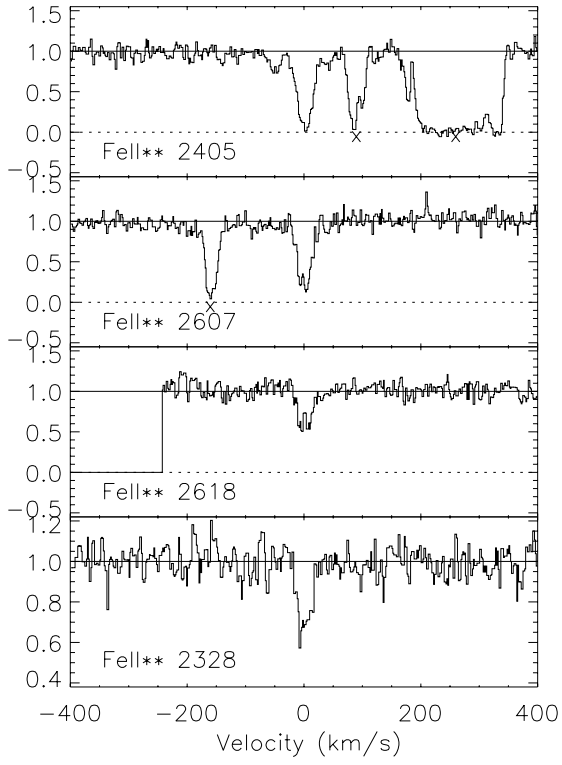

FIG. 7.—Same as Fig. 2, but for Fe II** transitions.

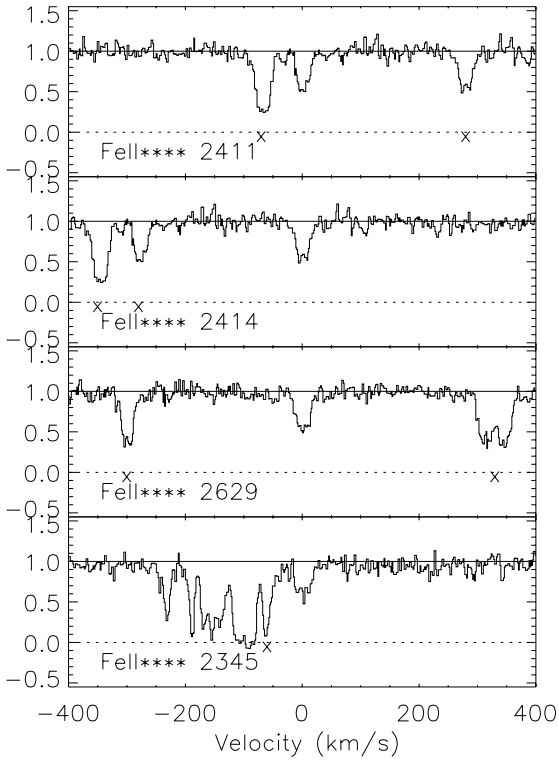

FIG. 9.—Same as Fig. 2, but for Fe II**** transitions.

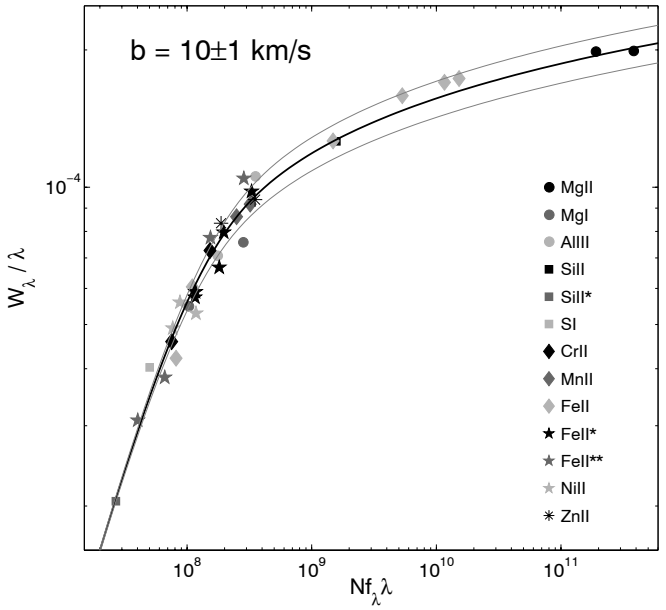

FIG. 10.—Curve of growth (COG) for the host galaxy system of GRB 051111. We constructed the COG by iteratively fitting for the column densities of individual ions and for the Doppler parameter, b, which we assumed to have a single value. Transitions in the linear part of the COG lead to well-determined columns. Transitions on the flat portion of the COG are sensitive to the value of b.

with the line center's optical depth, given by

$$\tau_0 = \frac{\pi^{1/2} e^2 f_\lambda \lambda N}{m_e c b} = 1.496 \times 10^{-15} \frac{f_\lambda (\lambda/\text{Å}) N}{(b/\text{km s}^{-1})}, \quad (2)$$

using the function

$$F(\tau_0) = \int_0^\infty [1 - \exp(-\tau_0 e^{-x^2})]\, dx. \quad (3)$$

Here f_λ is the oscillator strength, W_λ is the equivalent width, and λ is the rest wavelength, and we assume that all species share the same value of the Doppler parameter, b. We fit iteratively for b and the column density of each species (e.g., Savaglio et al. 2003). The resulting best-fit COG, with a Doppler parameter, $b \approx 10$ km s^{-1}, is shown in Figure 10, and the column densities are listed in Table 2.

From the combined COG analysis we note that the best-fit value of $b = 10$ km s^{-1} is comparable to the observed values of Ca II line widths for atomic filaments and translucent molecular clouds in our Galaxy (e.g., Penprase & Blades 2000; Penprase 1993), as well as for the well-studied sight lines of Zeta Oph, for which *HST* observations of ions ranging from Mg II to Zn II show absorption over a velocity range of 20 km s^{-1}, and structure with typical widths of approximately 5–10 km s^{-1} (Savage & Sembach 1996).

To obtain additional information on the column density velocity structure, $N(v)$, and the abundances of elements as a function of velocity, we also use the apparent optical depth method (Savage & Sembach 1991), where

$$N = \int N(v)\, dv = \frac{m_e c}{\pi e^2 f \lambda} \int \tau(v)\, dv, \quad (4)$$

and the optical depth

$$\tau(v) = \ln [I_0(v)/I(v)]. \quad (5)$$

This method has the advantage that it makes no a priori assumptions about the functional form of the velocity distribution, and at the same time it incorporates information from a wide variety of lines with different oscillator strengths. By combining the optical depths of these lines and eliminating the contribution from high optical depth and saturated velocity channels in the co-added velocity spectrum, an improved estimate of both the column density and the velocity structure of the line profile is obtained, which include a measurement of the velocity structure within the cores of the lines.

We apply the apparent optical depth technique to all of the detected absorbing species and summarize the resulting column densities in Table 2; the $N(v)$ profiles are shown in Figures 11–13. We also include in Table 2 the adopted column density for each species, which is either derived from the apparent optical depth approach or an average with the COG values, depending on

TABLE 2

COLUMN DENSITIES OF IONS IN z_1 COLUMN DENSITIES OF IONS IN z_1

ION	COG			AOD			ADOPTED		
	z_{1a}	z_{1b}	z_{1c}	z_{1a}	z_{1b}	z_{1c}	z_{1a}	z_{1b}	z_{1c}
Mg II	15.05	>14.78	13.59	14.22	>13.88	13.62	14.22 ± 0.08	>14.70	13.62 ± 0.08
Mg I	<13.6	14.85	<13.4	<13.26	14.72	<13.1	<13.3	14.72 ± 0.01	<13.1
Al III	<13.2	13.39	<12.4	13.05	13.34	<12.4	13.05 ± 0.20	13.34 ± 0.10	<12.4
Si II	...	...	...	14.13	16.18	<14.5	14.13 ± 0.10	16.18 ± 0.20	<14.5
Si II*	...	...	...	<14.1	14.96	<14.5	<14.1	14.96 ± 0.02	<14.5
S I	...	...	...	<12.3	13.50	<12.6	<12.3	13.50 ± 0.02	<12.6
Cr II	<13.2	13.80	<11.8	<12.9	13.85	<11.9	<12.9	13.85 ± 0.10	<11.9
Mn II	<10.4	13.84	<11.5	<10.4	13.52	<11.6	<10.4	13.52 ± 0.15	<11.6
Fe II	14.66	15.32	14.51	14.29	15.15	13.74	14.29 ± 0.10	15.15 ± 0.10	13.74 ± 0.10
Fe II*	<12.5	13.91	...	<12.2	13.90	<12.3	<12.2	13.90 ± 0.10	<12.3
Fe II**	<12.5	13.70	<12.2	<12.2	13.70	<12.0	<12.2	13.70 ± 0.08	<12.0
Fe II***	<12.5	13.54	<12.1	<12.2	13.52	<12.1	<12.2	13.53 ± 0.10	<12.1
Fe II****	<12.8	13.21	<12.0	<12.5	13.15	<12.0	<12.5	13.18 ± 0.10	<12.1
Ni II	<13.5	15.05	<12.9	<14.2	13.99	<12.8	<13.5	13.99 ± 0.35	<12.8
Zn II	<11.7	13.87	<11.9	<11.8	13.58	<12.0	<11.8	13.58 ± 0.15	<12.0

NOTES.—Ionic column densities and abundances as derived from the curve-of-growth analysis and apparent optical depth technique. The three velocity ranges are defined in § 4.

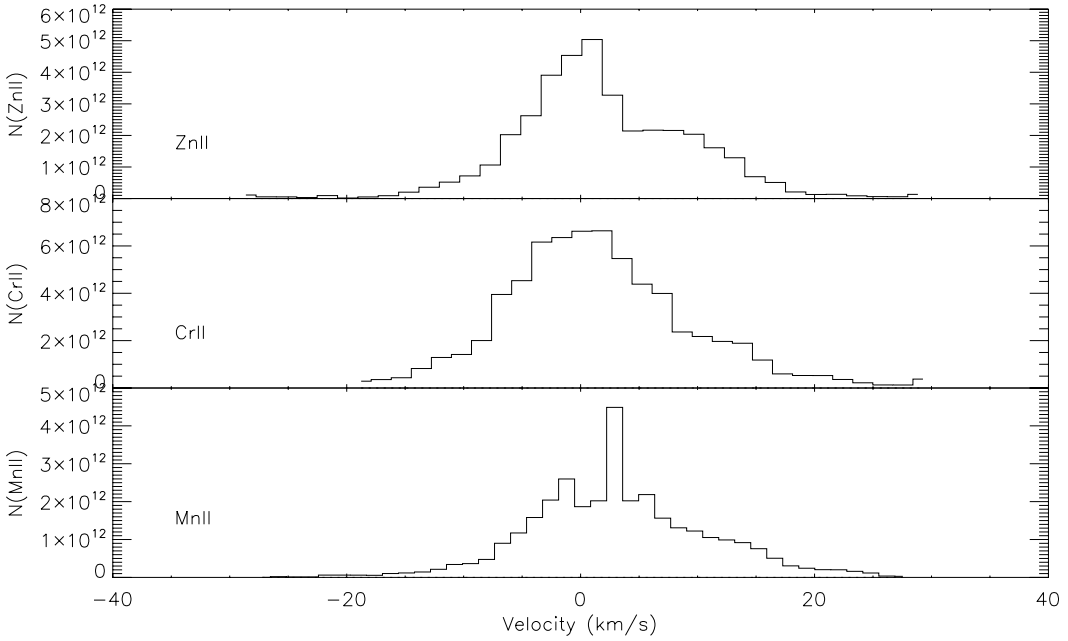

FIG. 11.—Stacked plot of $N(v)$ of the ions Zn II, Cr II, and Mn II, showing the strongly peaked and narrow component at -30 km s$^{-1} < v < 30$ km s^{-1}.

the number of transitions and degree of saturation. Using the shapes of the various lines we define three velocity ranges—z_{1a}: $v < -30$ km s^{-1}, z_{1b}: $-30 < v < +30$ km s^{-1}, and z_{1c}: $v > +30$ km s^{-1}—and determine the column densities in each range. This is particularly useful for the Fe II and Mg II, which exhibit a wide velocity range. We find that the dominant z_{1b} system accounts for about 85% of the Fe II column and $\gtrsim$70% of the Mg II column.

We estimate the neutral hydrogen column density using the column density of Zn II, since Zn is a nonrefractory iron peak element and its gas-phase abundance should therefore closely match the gas metallicity. Using a value of $\log N(\text{Zn II}) = 13.58 \pm 0.15$ and a typical metallicity of $[\text{Zn/H}] \approx -1$ for DLA systems at $z \sim z_1$ (Akerman et al. 2005), we derive $\log N(\text{H I}) \approx 21.9$, indicating a DLA systen with an H I column density that is similar to those of some other GRB absorption systems (e.g., Vreeswijk et al. 2004; Berger et al. 2006) and is significantly larger than those in typical QSO-DLA systems. This is not surprising since the Zn II column density exceeds the highest column densities measured in QSO-DLA systems by about 0.5 dex, and the median value by nearly 1.5 dex (Fig. 14). As we show below, the detailed abundance pattern of the main absorption component (z_{1b}) is markedly different from those in QSO-DLA systems and along with the large inferred value of $N(\text{H I})$ reflects the fact that it is a region of the ISM that is generally missed in quasar sight lines.

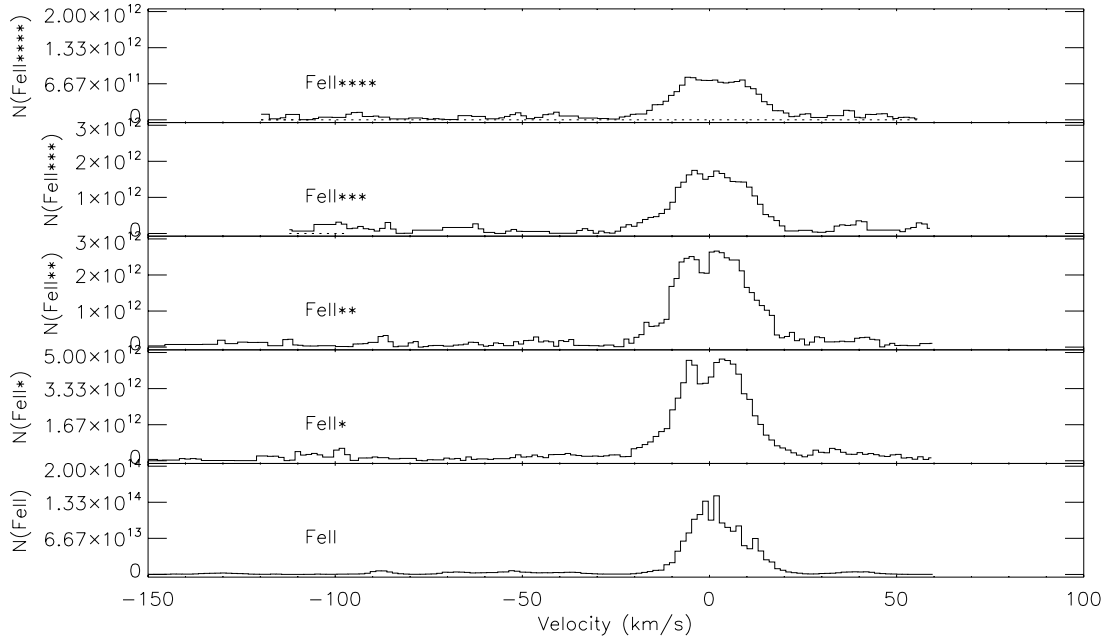

FIG. 12.—Stacked plot of $N(v)$ for the fine-structure excited Fe II levels within the main absorption system of GRB 051111, plotted across the entire velocity range of detected Fe II. The kinematics of the Fe II across the fine structure levels shows a strong and relatively narrow pair of peaks with slightly broader absorption in the higher excitation levels.

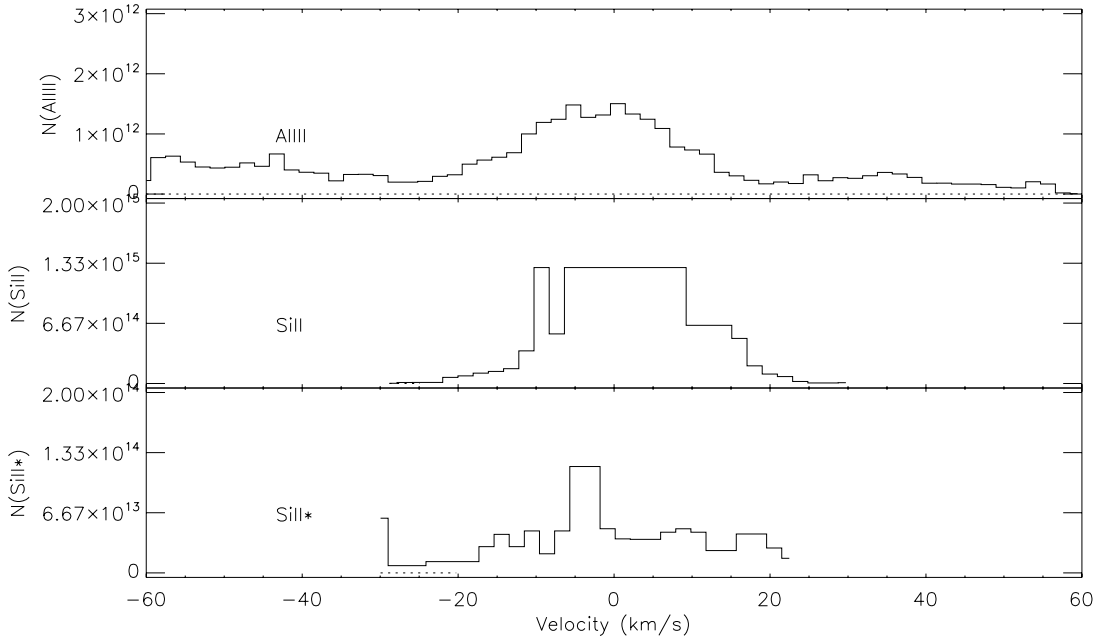

FIG. 13.—Stacked plot of $N(v)$ for the Al III, Si II, and Si II* within GRB 051111. The Si II line is saturated, and our resulting column density is a lower limit. The Si II* column density is clearly much weaker compared to the ground state than that observed in the case of Fe II.

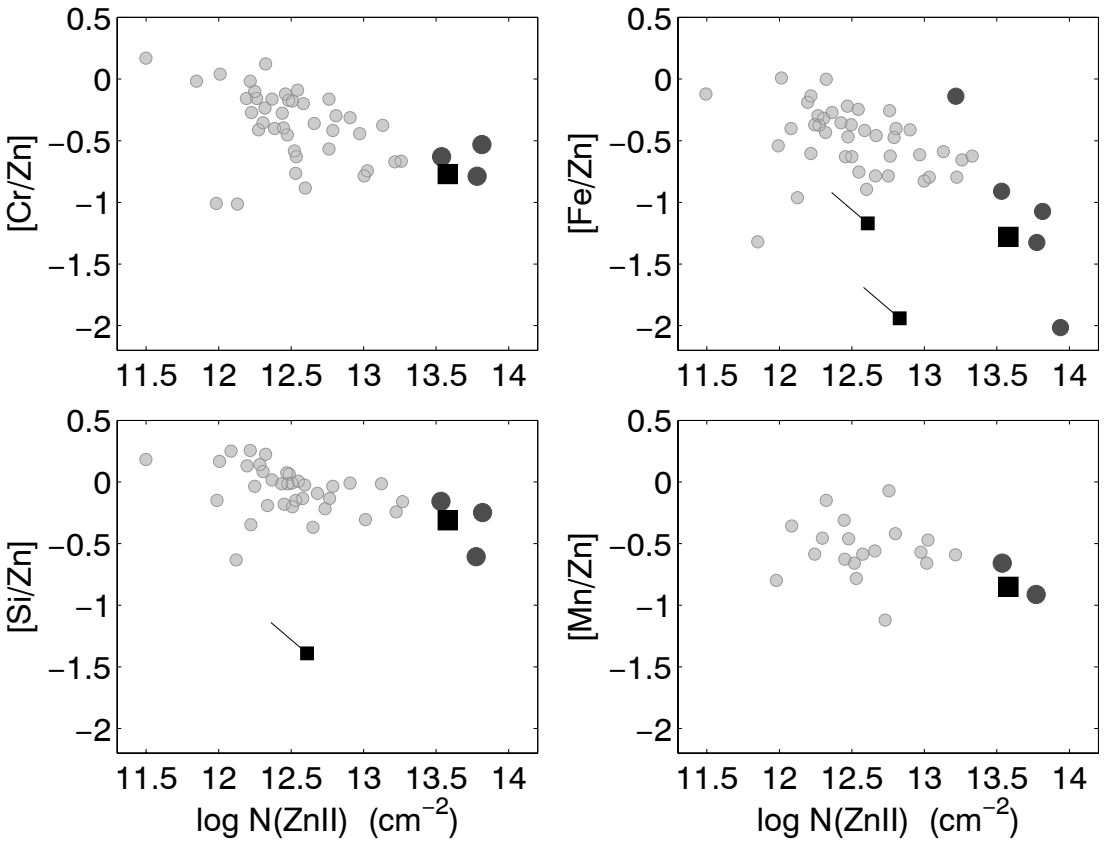

FIG. 14.—Column density ratios from GRB 051111 of various species compared to the nonrefractory Zn II (*squares*), along with the values for past GRB-DLA systems and for QSO-DLA systems (*circles*). The DLA sample is taken from Savaglio & Fall (2004) and is consistent with a newer DLA sample from the Keck HIRES spectrograph. Small squares show the range of values possible for absorption from the system at larger velocities outside the main -30 km s$^{-1} < v < 30$ km s^{-1}, and where we have lower limits, the ratios follow the vector indicated in the figure.

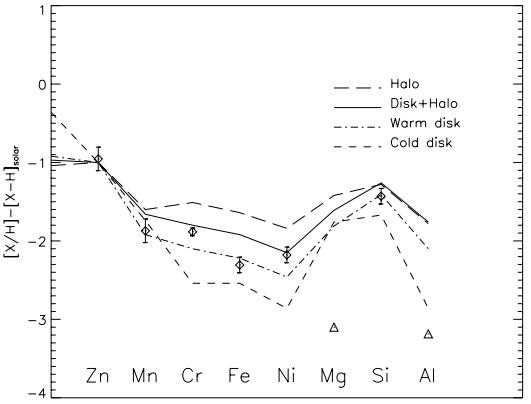

FIG. 15.—Depletion pattern for the main absorber (z_{1b}) in the host galaxy of GRB 051111. The pattern of depletion is typical for warm disk clouds such as those observed in the Milky Way (Savage & Sembach 1996). We have adopted a value of [Zn/H] ≈ -1 for the figure, and changes in the value of [Zn/H] will have the effect of shifting both the data points and models in the vertical axis.

However, it is impossible to rule out the possibility that a larger metal abundance could exist within the absorbing gas, in which [Zn/H] ≈ 0. Some evidence suggests that for DLA systems with [Zn/Fe] ≈ -1.3, the values of [Zn/H] approach solar abundances (Pettini 2004; Wolfe et al. 2005). In this case our derived H I column density would approach $\log N(\mathrm{H\ I}) \approx 20.9$, which we consider a lower limit. The lower column density would not affect our discussion of the abundance pattern but would have a significant impact on our estimated dust to gas ratio, which we include in the discussion below.

5. DEPLETION PATTERNS AND DUST WITHIN THE GRB 051111 HOST GALAXY

The difference in the velocity structure of various species, coupled with the expected difference in depletion for the nonrefractory (e.g., Zn) and refractory (e.g., Fe) elements, indicates that the sight line to GRB 051111 likely probes various components of the host galaxy's interstellar medium. We begin by investigating the main absorption component z_{1b}. The column density ratios of various species compared to the nonrefractory Zn II are shown in Figure 15, along with the values for past GRB-DLA systems and for QSO-DLA systems in Figure 14.

We find that for z_{1b} the Cr to Zn ratio is [Cr/Zn] $= -0.8 \pm 0.2$, which is at the low end of the distribution for QSO-DLA systems with $\langle$[Cr/Zn]$\rangle = -0.3 \pm 0.3$ (Fig. 14). Since Cr and Zn are produced in the same nucleosynthetic pathway, differences in the abundances of these elements arise from differential dust depletion. Similarly, the ratio [Fe/Zn] $= -1.3 \pm 0.2$ is significantly lower than that in QSO-DLA systems for which $\langle$[Fe/Zn]$\rangle = -0.5 \pm 0.3$. We find the same results for the ratios of Si and Mn relative to Zn. In all cases our elemental abundances are referenced relative to the solar values in Lodders (2003). Taken in conjunction with the unusually large Zn II column density compared to QSO-DLA systems, we conclude that the main absorption component is dense and strongly dust-depleted.

The large Zn II column density and strong depletion are remarkably similar to those measured in past GRB absorption systems (Savaglio & Fall 2004). This suggests that GRB sight lines probe similar regions at various redshifts, reflecting a possible uniformity in the environmental conditions that supports GRB progenitor formation and possibly star formation in general. Similarly, the strong dust depletion indicates that similar regions are missed in quasar sight lines, not just because of their small cross section but also because of the associated dust extinction.

Given that Zn is largely undepleted, we estimate the dust content along the sight line to GRB 051111 to be about 2.5 times higher than that in typical DLA gas but comparable, per unit metallicity, to Milky Way gas. Applying our adopted metallicity of 1/10 solar we find that the dust-to-gas ratio is approximately 1/12 that of Milky Way gas, scaling the relation described in Pettini (2004). With our estimated column density of $\log N(\mathrm{H\ I}) \approx 21.9$, we then expect about 0.55 mag of V-band extinction toward GRB 051111 using the relation $\langle N(\mathrm{H\ I})/Av\rangle = 1.5 \times 10^{21}$ cm^{-2} mag^{-1}, scaled for the lower metallicity estimated toward GRB 051111 (Diplas & Savage 1994). Using an SMC extinction curve appropriate for low-metallicity gas (Bouchet et al. 1985), we derive that the GRB 051111 sight line has an extinction of $A(1500) \sim 5.0$ mag in the rest frame UV.

Since our estimate of $\log N(\mathrm{H\ I}) \approx 21.9$ is based on metallicities typical for redshifts comparable to that of GRB 051111 and is not measured directly, it is not possible to rule out a larger Zn abundance. In the case of [Zn/H] ≈ 0, the resulting dust to gas ratio would approach that of Milky Way gas. The estimated V-band extinction would be unchanged since it is based on the column density of metals toward GRB 051111 but the resulting UV extinction could decrease substantially. Using a standard galactic extinction law (Savage & Mathis 1979), the resulting extinction of $A(1500) \sim 2.5$ mag would be estimated in the high-metallicity case.

As described in detail in Savage & Sembach (1996), depletion patterns can reveal the presence of warm and cold gas along the line of sight. The full depletion pattern for the z_{1b} component is shown in Figure 15 in comparison to the four typical patterns observed in the Milky Way of warm halo (WH), warm disk+halo (WDH), warm disk (WD), and cool disk (CD) clouds (Savage & Sembach 1996). We note that the Mg absorption lines are heavily saturated, and the inferred abundance is therefore a lower limit. Similarly, in the case of Al, only the Al III transition is observed, and we are therefore unable to account for any additional Al II gas. Taking these effects into account, we find that the observed abundances closely match the WD pattern, or marginally the WDH pattern. The more weakly depleted WH and the strongly depleted CD do not provide an adequate fit to the data. It should be emphasized that despite the fact that the value of $\log N(\mathrm{H\ I})$ is not known, the precise value of $\log N(\mathrm{H\ I})$ will not affect the conclusions, since changing $\log N(\mathrm{H\ I})$ will simply shift both the data and models vertically in Figure 15 and not change the conclusion that the gas follows the WD pattern.

So far we have discussed only the main component of the line absorption profiles, but it is clear from the different shape of the Fe II and Mg II lines compared to the other species that the depletion pattern changes across the line profile. We find that [Fe/Zn] > -1.9 (z_{1a}) and [Fe/Zn] > -1.2 (z_{1c}), along with the limits of $\log N(\mathrm{Zn\ II}) \lesssim 12.7$, are similar to those found in QSO-DLA systems (Fig. 14) but are different from the depleted z_{1b} component. This suggests that the sight line to GRB 051111 probes in addition to the dense component in the GRB local environment, a region in the halo of the host galaxy, which is typical of the sight lines probed by background quasars. Given the combination of kinematic structure and abundance patterns, we find that the GRB probably exploded away from the center of the galaxy, most likely in the spiral arm of a highly inclined disk.

6. FINE-STRUCTURE EXCITATION OF Fe II AND Si II

In addition to the various transitions discussed above, from which we deduce a warm and depleted environment in the z_{1b} absorber coincident with the GRB, we also detect absorption lines

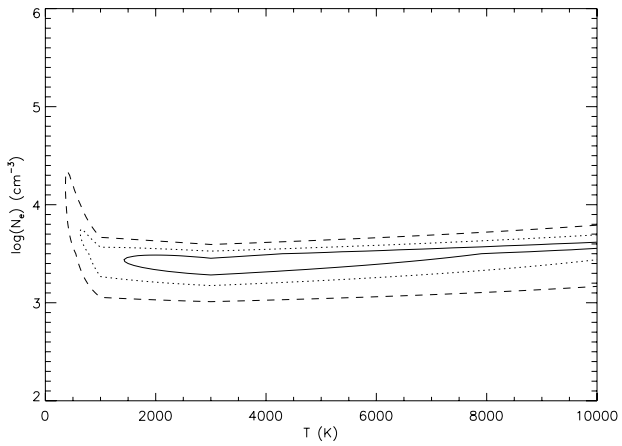

FIG. 16.—Reduced χ^2 contours for the Fe II fine-structure column densities compared to the ground-state compared with predictions from Keenan et al. 1988. The contours show values of $\chi^2_r = 1$ (*solid line*), 2 (*dotted line*), and 5 (*dashed line*), giving a range of possible density and temperature within the GRB 051111 absorber, assuming collisional excitation.

arising from all of the available ground-level fine-structure states of Fe II and Si II. A detailed analysis of these lines and the inferred physical conditions are summarized in a companion paper (Berger et al. 2005), but we investigate this here in the context of the inferred depletion pattern.

As shown in Figure 12, the velocity structure of the Fe II fine-structure levels is similar to that of the dense and depleted component, z_{1b}. The Si II* transition is weaker and as a result the velocity structure is not clear, but the strongest absorption arises from $v \approx 0$ km s^{-1} (Fig. 12). We use the apparent optical depth method over the full velocity range of $|v| < 30$ km s^{-1} to derive the column densities of the fine-structure states (see Table 2). We find that $\log N(\mathrm{Si\ II}^*) = 14.96$ is somewhat higher than the column densities measured in GRB 050505 ($\log N \approx 14.7$; Berger et al. 2006), GRB 030323 ($\log N \approx 14.2$; Vreeswijk et al. 2004), and GRB 020813 ($\log N \approx 14.3$; Savaglio & Fall 2004).

The excitation of the fine-structure levels requires either a combination of a high temperature and a high gas volume density, or an intense IR or UV radiation field. The radiation field may be due to the GRB itself, but in the case of excitation by the ambient radiation field due to star formation activity, the inferred luminosity and size of the region would naturally lead to a warm, dust-depleted environment.

In particular, excitation of the fine-structure levels by an IR radiation field, along with the observed ratios of the Fe II and Si II fine-structure levels, are indicative of a warm dust spectrum, $F_\nu \propto \nu^{2.2}$ with $T \gtrsim 600$ K. The alternative interpretation of collisional excitation similarly leads to a large electron volume density, $n_e \gtrsim 10^3$ cm^{-3}, and temperature, $T_e \sim 10^3$ K (Fig. 16). In both scenarios we expect that the depletion pattern would be similar to that of a warm disk environment, and with a significant depletion.

7. GRB HOST GALAXY IMAGING

In an attempt to place the information from the absorption spectrum of GRB 051111 in the overall context of the host galaxy properties, we observed the position of the burst with the Echellete Spectrograph and Imager (ESI) mounted on the Keck II telescope on 2005 November 30. A total of 1500 s were obtained in R band. At the position of the afterglow we detect a faint extended source that we identify as the host galaxy (Fig. 17). A comparison to two nearby and unsaturated stars in the USNO-B catalog indicates a brightness of $R = 26 \pm 0.3$ mag for this object. At the

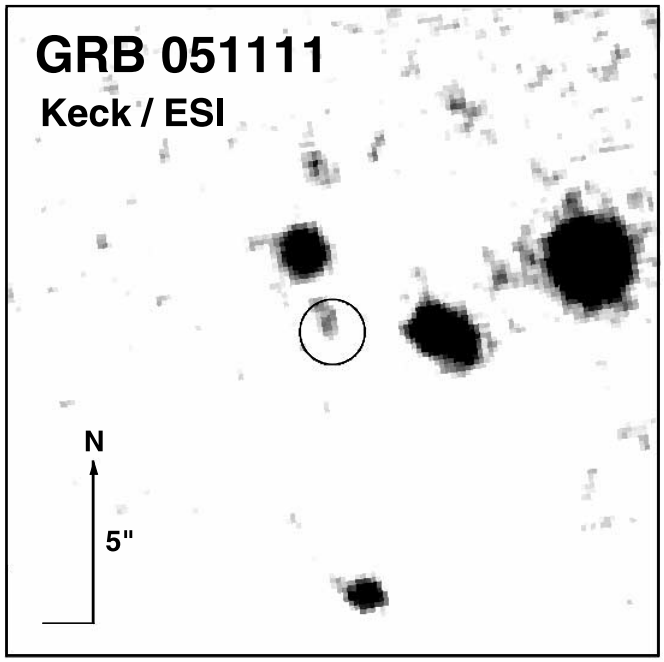

FIG. 17.—Keck ESI image of the field near GRB 051111, showing the error circle of the coordinates for the GRB 051111 (*circle*) and two adjacent galaxies probably responsible for the intervening Mg II and Fe II absorption lines seen at lower redshifts of $z_2 = 1.18975$, $z_{3a} = 0.82761$, and $z_{3b} = 0.82698$. The 2″–3″ offset from the centers of these adjacent galaxies amounts to a distance from the center of the galaxy of 15–20 kpc.

redshift z_1 and assuming a spectrum $F_\nu \propto \nu^{-1}$, this translates to an absolute rest-frame B-band magnitude of about -18.6, or $L \approx 0.1L^*$. This value is similar to that of other GRB host galaxies that at a similar redshift range from about -17 to -21 mag.

Since the observed R band probes the rest-frame UV emission from the host galaxy, we can roughly estimate the star formation rate in the host galaxy. Using the relation of Kennicutt 1998, $\mathrm{SFR} = 1.4 \times 10^{-28} L_\nu$, we find that SFR $\approx 3\ M_\odot$ yr^{-1}. Clearly, this value is subject to a large upward correction due to possible dust extinction. If the estimated extinction provided above based on the depletion pattern in the GRB local environment is representative, then it is possible that the star formation rate easily exceeds 30 $M_\odot$ yr^{-1}.

8. INTERVENING SYSTEMS

Within the spectrum of GRB 051111 we detect intervening absorption systems at $z_2 = 1.18975$ from absorption by Mg II, Mg I, and Fe II. The column densities for these systems derived from optical depth and COG fitting of the absorption lines are $\log N(\mathrm{Mg\ II}) = 14.33 \pm 0.05$, $\log N(\mathrm{Mg\ I}) = 12.58 \pm 0.1$, and $\log N(\mathrm{Fe\ II}) = 14.31 \pm 0.05$. An additional pair of absorption systems are seen at $z_{3a} = 0.82761$ and $z_{3b} = 0.82698$ in the species Mg I, Mg II, and Fe II. For the absorption system at $z_{3a} = 0.82761$, we estimate column densities of $\log N(\mathrm{Mg\ II}) = 13.28 \pm 0.1$, $\log N(\mathrm{Mg\ I}) = 12.38 \pm 0.1$, and $\log N(\mathrm{Fe\ II}) = 12.95 \pm 0.05$. The column densities of the absorption lines at $z_{3b} = 0.82698$ are $\log N(\mathrm{Mg\ II}) = 13.1 \pm 0.15$ and $\log N(\mathrm{Fe\ II}) = 12.70 \pm 0.05$.

Bowen et al. (1995) conducted a survey of Mg II absorption from the disks and halos of 17 low-redshift galaxies and studied the correlation between the impact parameter, ρ, and the line equivalent width. The sample includes a range of $\rho \approx 2$–113 kpc, and equivalent widths from 0.05 to 2 Å. Systems with Mg II equivalent widths >0.1 Å appear to have smaller impact parameters, $\rho < 20$–30 kpc, while the largest impact parameter

systems are seen to have much smaller equivalent widths. The z_2 and z_3 intervening systems in the spectrum of GRB 051111 exhibit equivalent widths of 1.7 and 0.2 Å, respectively. Thus, both of these intervening systems are at the high end of the Bowen et al. (1995) sample, indicating small impact parameters.

Our image of the field of GRB 051111 reveals two nearby galaxies, which are significantly brighter than the GRB host, one located 2″ to the north and the other about 2.″5 to the west (Fig. 17). While we do not have redshifts for these galaxies, it is likely that they are responsible for the intervening systems z_2 and z_{3ab}. The derived impact parameters relative to the GRB position are about 17 and 20 kpc, indicating that the intervening absorbers are similar to those found by Bowen et al. (1995).

9. DISCUSSION AND CONCLUSIONS

The high-resolution spectrum of GRB 051111 reveals a range of interstellar abundance patterns within the host galaxy. In addition to warm halo gas, which is typical of quasar sight lines and represents the bulk of the galaxy cross section, we detect a high column density, kinematically cold region of dust-depleted gas, which is typical of a warm disk abundance pattern. The observed abundance pattern in this component is similar to those in several other GRB absorption spectra obtained in the past. The weaker Fe and Mg absorption with a wider positive and negative velocity extension of several hundred km s^{-1} suggests that the GRB location was offset from the center of the galaxy. While the Lyα line is not detected in our spectrum, a reasonable value of the metallicity $Z \sim 0.1\ Z_{\odot}$, combined with a large Zn II abundance, indicates that the host is likely a DLA system with $\log N(\mathrm{H\ I}) \approx 21.9$, higher than typical QSO-DLA systems but in good agreement with other GRB-DLA systems (Vreeswijk et al. 2004; Berger et al. 2006; Chen et al. 2005).

The detection of strong absorption from Fe II and Si II fine-structure levels (discussed in detail in Berger et al. 2005) requires physical conditions that are in good agreement with the conclusion that the local environment is warm and dust-depleted. In the case of collisional excitation, the inferred temperature is about 10^3 K, while in the case of IR pumping dust reprocessing is probably essential for generating the required IR radiation field.

We finally identify the host galaxy and the likely counterparts of the two intervening systems detected in the spectrum. As in the case of previous GRB hosts, the galaxy is relatively faint, $L \sim 0.1L^*$. A comparison of the Mg II column densities of the intervening systems with the offsets of the two nearby galaxies relative to the GRB position is in good agreement with previous correlations with impact parameters found in the context of quasar studies. If the intervening systems occurred at a higher redshift in which we could determine directly whether they are DLA systems, one can imagine that similar imaging, as well as follow-up spectroscopy, would provide direct insight into the nature of DLA systems, a question that remains difficult to address in the context of QSO-DLA sytems.

B. E. P. would like to thank Pomona College for support from a Downing Exchange fellowship to Cambridge University, and would like to thank Max Pettini, Edward Jenkins, Jason Prochaska, and Bruce Draine for helpful discussions. E. B. is supported is supported by NASA through Hubble Fellowship grant HST 01-171.01 awarded by the Space Telescope Science Institute, which is operated by Association of Universities for Research in Astronomy (AURA), Inc., for NASA under contract NAS 5-26555.

REFERENCES

Akerman, C. J., Ellison, S. L., Pettini, M., & Steidel, C. C. 2005, A&A, 440, 499
Albert, C. E., Blades, J. C., Morton, D. C., Lockman, F. J., Proulx, M., & Ferrarese, L. 1993, ApJS, 88, 81
Berger, E., Penprase, B. E., Cenko, S. B., Kulkarni, S. R., Fox, D. B., Steidel, C. C., & Reddy, N. A. 2006, ApJ, 642, 979
Berger, E., Penprase, B. E., Fox, D. B., Kulkarni, S. R., Hill, G., Schaefer, B., & Reed, M. 2005, ApJ, submitted (astro-ph/0512280)
Bloom, J. S., Kulkarni, S. R., & Djorgovski, S. G. 2002, AJ, 123, 1111
Bouchet, P., Lequeux, J., Maurice, E., Prevot, L., & Prevot-Burnichon, M. L. 1985, A&A, 149, 330
Bowen, D. V., Blades, J. C., & Pettini, M. 1995, ApJ, 448, 634
Bunker, A. J., Warren, S. J., Clements, D. L., Williger, G. M., & Hewett, P. C. 1999, MNRAS, 309, 875
Castro, S., Galama, T. J., Harrison, F. A., Holtzman, J. A., Bloom, J. S., Djorgovski, S. G., & Kulkarni, S. R. 2003, ApJ, 586, 128
Chen, H.-W., Prochaska, J. X., & Bloom, J. S. 2006, preprint (astro-ph/0602144)
Chen, H.-W., Prochaska, J. X., Bloom, J. S., & Thompson, I. B. 2005, preprint (astro-ph/0508270)
Diplas, A., & Savage, B. D. 1994, ApJ, 427, 274
Ellison, S. L., Mallén-Ornelas, G., & Sawicki, M. 2003, ApJ, 589, 709
Hill, G., Prochaska, J. X., Fox, D., Schaefer, B., & Reed, M. 2005, GCN Circ. 4255, http://gcn.gsfc.nasa.gov/gcn/gcn3/4255.gcn3
Keenan, F. P., Hibbert, A., Burke, P. G., & Berrington, K. A. 1988, ApJ, 332, 539
Kennicutt, R. C., Jr. 1998, ARA&A, 36, 189
Krimm, H., et al. 2005, GCN Circ. 4260, http://gcn.gsfc.nasa.gov/gcn/gcn3/4260.gcn3
Lodders, K. 2003, ApJ, 591, 1220
Möller, P., Warren, S. J., Fall, S. M., Fynbo, J. U., & Jakobsen, P. 2002, ApJ, 574, 51
Möller, P., et al. 2002, A&A, 396, L21
Morton, D. C. 1991, ApJS, 77, 119
Nagamine, K., Springel, V., & Hernquist, L. 2004, MNRAS, 348, 435
Penprase, B. E. 1993, ApJS, 88, 433
Penprase, B. E., & Blades, J. C. 2000, ApJ, 535, 293
Pettini, M. 2004, in Cosmochemistry: The Melting Pot of the Elements, ed. C. Esteban (Cambridge: Cambridge Univ. Press), 257
Prochaska, J. X. 2005, GCN Circ. 4271, http://gcn.gsfc.nasa.gov/gcn/gcn3/4271.gcn3
Prochaska, J. X., Gawiser, E., Wolfe, A. M., Cooke, J., & Gelino, D. 2003, ApJS, 147, 227
Rujopakarn, W., Swan, H., Rykoff, E. S., & Schaefer, B. 2005, GCN Circ., 4247 http://gcn.gsfc.nasa.gov/gcn/gcn3/4247.gcn3
Savage, B. D., & Mathis, J. S. 1979, ARA&A, 17, 73
Savage, B. D., & Sembach, K. R. 1991, ApJ, 379, 245
———. 1996, ARA&A, 34, 279
Savaglio, S., & Fall, S. M. 2004, ApJ, 614, 293
Savaglio, S., Fall, S. M., & Fiore, F. 2003, ApJ, 585, 638
Spitzer, L. 1978, Physical Processes in the Interstellar Medium (New York: Wiley)
Starling, R. L. C., et al. 2005, A&A, 442, L21
Vreeswijk, P. M., et al. 2004, A&A, 419, 927
Wolfe, A. M., Gawiser, E., & Prochaska, J. X. 2005, ARA&A, 43, 861